On Kinetic Mechanisms of n-Decane Oxidation

Article *in* Combustion Explosion and Shock Waves · March 2011

DOI: 10.1134/S0010508211020018

CITATIONS
11

READS
258

3 authors:

Nataliya Titova
Central Institute of Aviation Motors
164 PUBLICATIONS **1,286** CITATIONS
SEE PROFILE

Sergey Torokhov
Central Institute of Aviation Motors
14 PUBLICATIONS **26** CITATIONS
SEE PROFILE

Alexander Starik
Central Institute of Aviation Motors
399 PUBLICATIONS **2,077** CITATIONS
SEE PROFILE

Combustion, Explosion, and Shock Waves, Vol. 47, No. 2, pp. 129–146, 2011

On Kinetic Mechanisms of *n*-Decane Oxidation

N. S. Titova,[1] S. A. Torokhov,[1] and A. M. Starik[1]

UDC 541.124

Translated from *Fizika Goreniya i Vzryva*, Vol. 47, No. 2, pp. 3–22, March–April, 2011.
Original article submitted March 9, 2010.

A kinetic model is built to describe ignition and pyrolysis of *n*-decane. The model involves 1021 reversible reactions and 144 species and includes both the high-temperature and low-temperature oxidation mechanisms. The model is tested against experimental data on the ignition delay time, changes in the concentration of OH radicals behind the reflected shock wave, and evolution of various species during *n*-decane pyrolysis in a flow reactor in a wide range of temperatures ($T = 650$–1640 K), pressures ($p = 1$–80 atm), and equivalence ratios ($\phi = 0.5$–3). This kinetic model ensures a more accurate description of experimental data on the ignition delay time than other known kinetic models, especially at low initial temperatures.

Keywords: ignition, combustion, heavy hydrocarbons, low-temperature mechanism, kinetic model.

INTRODUCTION

Much attention is currently paid to studying specific features of ignition and combustion of heavy hydrocarbons in air mixtures. This interest is caused by the necessity of detailed understanding of combustion processes in combustion chambers of various devices, beginning from power engineering facilities operating on organic fuels and ending with aircraft and rocket engines. It should be noted that, owing to recent investigations, it became possible to develop kinetic mechanisms to describe ignition and combustion of both simple hydrocarbons (methane, ethane, ethylene [1–4]) and more complex hydrocarbons (propane, butane, heptane, octane, decane, and dodecane [5–14]), and even for fuels used in aviation engines and consisting of a large number of saturated and aromatic hydrocarbons [15–17]. Though significant progress has been reached in this field and the reaction mechanisms developed provide a satisfactory description of experimental data on the ignition delay and flame propagation velocity, many issues have not been elucidated yet. Thus, for instance, for hydrocarbons such as *n*-propane and *n*-decane, there is no quantitative agreement between the calculated and measured ignition delay times at comparatively low temperatures ($T < 1000$ K); the so-called cold-flame phenomena have not been adequately understood. Moreover, the majority of the published mechanisms for heavy hydrocarbons, such as *n*-decane and *n*-dodecane, do not include reactions typical for low-temperature oxidation of alkanes at all.

Particular attention in the analysis of the oxidation kinetics of heavy alkanes C_nH_{2n+2} ($n \geqslant 8$) is paid to *n*-decane. The point is that, first, *n*-decane is included in almost all surrogates modeling real fuels for aviation and rocket engines [15–18]. Moreover, the kinetics of *n*-decane oxidation is often used to approximate the kinetics of ignition and combustion of aviation kerosenes [15, 19, 20]. In addition, the kinetic mechanism of *n*-decane oxidation serves as a basis for developing reaction mechanisms of ignition and combustion of heavier alkanes: *n*-$C_{12}H_{26}$, *n*-$C_{14}H_{30}$, and *n*-$C_{16}H_{34}$ [21]. It is for this reason that most experimental data for heavy alkanes obtained recently at both high and low temperatures mainly refer to the process of *n*-decane ignition and combustion [22–29]. Many publications deal with the development of various reaction mechanisms for the description of *n*-decane ignition and combustion in air or oxygen [13–15, 18, 21, 30–32]. Even the latest detailed kinetic models [18, 21, 31, 32], however, do

[1]Baranov Central Institute of Aviation Motors, Moscow 111116; star@ciam.ru.

0010-5082/11/4702-0129

not provide an accurate description of experimentally measured ignition delay times in shock tubes [27, 28] at comparatively low temperatures ($T_0 < 1000$ K).

At the moment, all existing kinetic models of combustion of alkanes can be classified as follows: detailed, lumped, reduced, skeleton, and global models.

Detailed models usually include all elementary processes and contain (for heavy alkanes i-C_8H_{18}, n-$C_{10}H_{22}$, and n-$C_{12}H_{26}$) several thousands of reversible reactions with participation of hundreds species [21]. The construction of detailed kinetic reaction mechanisms, however, faces difficulties due to uncertainty of rate constants of some reactions, especially those with participation of isomers, and to necessity of choosing reactions responsible for the development of a chain process with participation of derivatives of the initial hydrocarbons. In addition, it is next to impossible to perform three-dimensional calculations of combustion in real devices with detailed kinetic mechanisms. Such reaction mechanisms are currently used only in combustion calculations with the simplest reactor models [33, 34].

In lumped kinetic models, reactions with various isomers of derivatives of heavy hydrocarbons are usually neglected, which allows the number of participants of chemical reactions to be reduced (to 100–150), but the basic characteristics of the process (induction time, heat release time, evolution of temperature and concentrations of the basic species, and final values of combustion parameters) can still be predicted rather accurately. These models can be used for two-dimensional calculations of ignition and combustion in reacting flows and in model devices [35–37].

Reduced models are constructed on the basis of detailed and lumped models and contain a limited number of reactions of principal importance for oxidation of a hydrocarbon considered, with participation of a moderate number of species. Thus, for instance, Patel et al. [38] constructed a reduced model for n-heptane combustion, which contains only 52 reactions and 29 species. Special methods of reduction of detailed (or lumped) reaction mechanisms, which allow kinetic scheme reduction in a fairly wide range of conditions and parameters of the mixture, have been developed [39, 40].

The so-called skeleton kinetic models are, actually, another version of reduced mechanisms, with the only difference that such models unite classes of reactions determining the evolution of the chain mechanism. Various stages of the process can include both elementary and global reactions. Such models offer fairly accurate predictions of the ignition and combustion times in the case of process initiation by gas compression (analog of the process in diesel engines) [41, 42]. The kinetic scheme applied in such calculations contains only 69 reactions with participation of 45 species.

Finally, the global kinetic models most widely used now for three-dimensional calculations of combustion processes in combustion chambers of real devices include only several basic species participating in global (united) reactions whose rate constants are determined on the basis of comparisons of the calculated results with experimental data [43, 44]. Such models, however, ensure a satisfactory description of high-temperature ignition and combustion only, though some attempts to take into account the low-temperature mechanism of ignition in such global models have been also made.

It should be emphasized once again, however, that all simplified models are developed on the basis of detailed or lumped reaction mechanisms and do not allow the evolution of the chain process of alkane oxidation to be retraced in a wide range of parameters and compositions of the mixture. Therefore, the principal attention is currently paid to the development of detailed and lumped reaction mechanisms for the description of oxidation and pyrolysis of heavy alkanes [14, 18, 21[.

This paper is aimed at developing a lumped mechanism of oxidation and pyrolisis of n-$C_{10}H_{22}$, which would describe both the low-temperature and high-temperature stages of the oxidation and ignition processes with sufficiently high accuracy. The mechanism was validated against shock-tube experimental data on the ignition delay time and evolution of OH radicals and on the evolution of species concentrations in a flow reactor.

KINETIC MODEL

The reaction mechanism developed in this work is based on the authors' previous studies [6, 10, 45] and includes all stages necessary to describe oxidation of heavy alkanes C_nH_{2n+2} [8–10]. It includes 1021 reactions and 144 species and involves both the low-temperature and high-temperature mechanisms of alkane oxidation. The diagram of chemical transformations forming the basis for this kinetic mechanism is shown in Fig. 1. The following notation is used here and in what follows: RH = C_nH_{2n+2}, R = C_nH_{2n+1}, Q = C_nH_{2n}, and Q$^{\cdot}$ = C_nH_{2n-1}; aldehydes are molecules containing the —CHO group, for example, CH_2O, CH_3CHO, C_3H_5CHO, etc.; ketones are molecules containing the —C—CO—C— group; ketyl-radicals are molecules containing the —C$^{\cdot}$=O group, for instance, CHO, CH_3CO, C_2H_5CO, etc. The list of the basic classes of reactions included into this kinetic mechanism is given below:

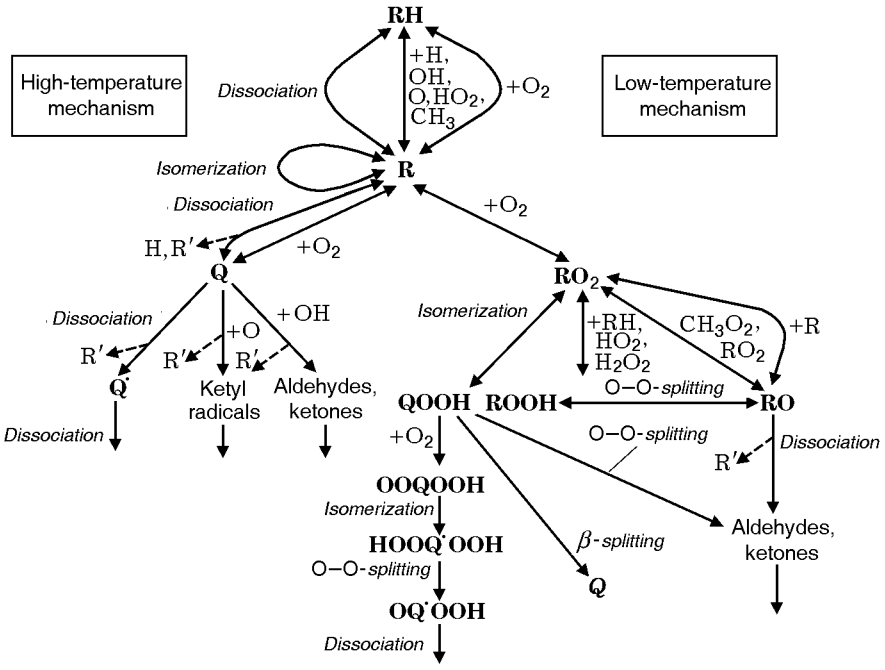

Fig. 1. Diagram of the chain process of n-decane oxidation.

1) monomolecular dissociation of alkane: RH = R′ + R″, RH = R + H;
2) abstraction of the H atom from alkane: RH+X = R + HX, X = H, O, OH, CH_3, HO_2, and O_2;
3) isomerization of the alkyl radical: $R_1 = R_2$;
4) dissociation of the alkyl radical: R = R′ + Q, R = H + Q;
5) oxidation of the alkyl radical: $R + O_2 = Q + HO_2$;
6) dissociation of alkene: $Q = R + Q^{\cdot}$;
7) interaction of alkenes with O atoms and OH radicals;
8) addition of the O_2 molecule to the alkyl radical: $R + O_2 = RO_2$;
9) isomerization of the alkyl-peroxide radical: RO_2 = QOOH;
10) addition of the O_2 molecule to the alkyl-hydroperoxide radical: $QOOH + O_2 = OOQOOH$;
11) isomerization of the OOQOOH radical: $OOQOOH = HOOQ^{\cdot}OOH$;
12) splitting of the O—O bond in the alkyl-hydroperoxide radical: $HOOQ^{\cdot}OOH = OQ^{\cdot}OOH + OH$;
13) dissociation of the $OQ^{\cdot}OOH$ radical;
14) dissociation of the alkyl-hydroperoxide radical: $QOOH = Q + HO_2$;
15) splitting of the O—O bond in the alkyl-hydroperoxide radical: QOOH = QO + OH;
16) interaction of QO with the OH and HO_2 radicals;
17) abstraction of the H atom by the alkyl peroxide from alkane: $RO_2 + RH = ROOH + R$;
18) interaction of the alkyl-peroxide radical with HO_2 and H_2O_2: $RO_2 + HO_2 = ROOH + O_2$, $RO_2 + H_2O_2 = ROOH + HO_2$;
19) splitting of the O—O bond in hydroperoxide ROOH = RO + OH;
20) interaction of the alkyl-peroxide radical with CH_3O_2 and RO_2: $RO_2 + CH_3O_2 = RO + CH_3O + O_2$, $RO_2 + RO_2 = RO + RO + O_2$;
21) abstraction of the O atom by the alkyl radical from the alkyl-peroxide radical: $RO_2 + R = RO + RO$;
22) dissociation of the unstable RO radical.

Note that the above-given classes of reactions are common for all n-alkanes and are partly included into the kinetic models used to describe cyclic and aromatic hydrocarbons [46, 47]. Table 1 gives a list of reactions with participation of n-$C_{10}H_{22}$ and its derivatives, as well as the coefficients for calculating the rate constants of forward and backward reactions $k_{+(-)q}$ by the Arrhenius formula $k_q(T) = A_q T^{n_q} \exp(-E_q/T)$, where A_q is the pre-exponential factor, E_q is the activation energy of the qth reaction, T is the gas temperature, and n_q is the temperature exponent. The coefficients for calculating $k_{+(-)q}$, which are listed in Table 1, were chosen on the basis of recommendations reported in [15,

16, 32, 47]. Some rate constants were taken for the given class of reactions to have the same value as for lighter alkanes and their derivatives (by the principle of "analogy"). Note that this principle is widely utilized for constructing kinetic models of oxidation and pyrolysis of heavy alkanes C_nH_{2n+2} ($n > 7$) [8–16, 21, 30–32]. The rate constants of the backward reactions not listed in Table 1 were calculated on the basis of the principle of detailed equilibrium balancing. Thermodynamic data necessary for calculations were taken from [47, 48]. The enthalpies of formation for the compounds $C_{10}H_{21}O_2$, $C_{10}H_{20}OOH$, $OOC_{10}H_{20}OOH$, $OC_{10}H_{19}OOH$, $C_{10}H_{21}O$, $C_{10}H_{21}OOH$, and $C_{10}H_{20}O$ were estimated by the method of additive groups [49]. For instance, the energy of the C—O bond in the $C_{10}H_{21}O_2$ molecule was assumed to be equal to the bonding energy in the $C_8H_{17}O_2$ molecule, and its value was determined by comparing the enthalpies of formation of the C_8H_{17} and $C_8H_{17}O_2$ molecules.

Oxidation of alkanes begins from their monomolecular decomposition or dissociation and H atom abstraction. The reactions of monomolecular decomposition of alkanes (class 1) with formation of alkyl radicals R are exothermic processes. Because of the high activation energy, the role of these reactions is significant only at high temperatures. Abstraction of the H atom from alkane during its interaction with various radicals or with the O_2 molecules, leading to formation of the alkyl radical (class 2), occurs at both high and low temperatures. Five different alkyl radicals can be formed from *n*-decane, depending on the position of the carbon atom that loses the H atom in the course of its abstraction. The rate constants of these reactions depend on the position of the abstracted H atom in the hydrocarbon molecule. As a result of isomerization of the alkyl radical (class 3), the H atom changes its displacement in the molecule, which is due to the existence of a free radical bond.

Further paths of alkyl radical transformation depend on temperature. Dissociation of the alkyl radical (class 4) with formation of the H atom or a smaller alkyl radical R′ and alkene Q (molecules with double bonds) proceeds over the bond in the β-position relative to the free radical bond (the so-called β-splitting). This reaction dominates at comparatively high temperatures ($T > 1000$ K) because of the appreciably high activation energy of this process. Oxidation of the alkyl radical with alkene formation (class 5) occurs simultaneously. To reduce the number of reagents, alkenes Q and species formed in the course of reactions with alkenes, having an identical chemical formula, and containing identical functional groups, are considered in this model as one individual species without separation into different isomers, i.e., a certain generalized sole alkene is formed from any identical alkyl radicals. This reaction can be written as $kC_{10}H_{21} + O_2 = C_{10}H_{20} + HO_2$ ($k = 1, \ldots, 5$). The same approach was utilized to reduce the processes with alkyl-peroxide radicals RO_2: $kC_{10}H_{21} + O_2 = C_{10}H_{21}O_2$. Thus, the species QOOH and OOQOOH formed in reactions from RO_2 were not classified as different isomers. Such an approach allows the number of species included into the reaction mechanism to be substantially reduced. For instance, the number of $C_{10}H_{20}OOH$ isomers formed by intramolecular isomerization from $C_{10}H_{21}O_2$ is as large as 30, if transitional states consisting of five, six, seven, and eight atoms in the ring are taken into account. Note that such a procedure lumpening the kinetic model was used in [32]. After that, alkenes dissociate (class 6) or interact with the O atom (class 7) with formation of smaller alkyl radicals and various oxo-compounds.

At $T < 1000$ K, the most important process is interaction of the alkyl radical with the oxygen molecule, leading to formation of the alkyl-peroxide radical RO_2 (class 8), which is also considered in our model as one species. This reaction is exothermic, but its activation energy is not too high. With increasing temperature, the alkyl-peroxide radical RO_2 rapidly dissociates into the alkyl radical and O_2. At low temperatures, RO_2 is subjected to the following consecutive processes: intramolecular isomerization (class 9), addition of the second O_2 molecule (class 10), and second intramolecular isomerization (class 11). After that, three radicals are formed in consecutive dissociation reactions (classes 12 and 13). As a result, three radicals, which are carriers of the chain mechanism, are formed from one alkyl radical. Thus, process No. 8 is the most important process of chain branching during low-temperature oxidation of alkanes. On the other hand, RO_2 can interact with HO_2 (class 18), forming a fairly stable hydroperoxide ROOH. This reaction is a reaction of chain termination and decreases the oxidation rate. This process, however, is bimolecular, and its rate depends on the concentration of HO_2 and usually is not very high. As a result, monomolecular isomerization of the radical RO_2 (class 9) proceeds much faster than its interaction with HO_2 (class 18). Therefore, the concentration of the hydroperoxide ROOH is rather low.

Another important process is interaction of the radical RO_2 with H_2O_2 (class 18). In the course of this reaction, the stable molecule of hydrogen peroxide H_2O_2 and the alkyl-peroxide radical RO_2 transform to another stable species ROOH and hydrogen dioxide HO_2. As the ROOH dissociation rate at low temperatures is higher than the rate of reactions with H_2O_2, the total reactivity of the system increases at low temperatures.

TABLE 1

Reactions with Participation of n-$C_{10}H_{22}$ and Its Derivatives and Corresponding Rate Constants

No.	Reaction	k_{+q}			k_{-q}		
		A_q, cm, mole, sec	n_q	E_{aq}, K	A_q, cm, mole, sec	n_q	E_{aq}, K
1	n-$C_{10}H_{22} = C_7H_{15} + nC_3H_7$	$7.85 \cdot 10^{14}$	0	34,146			
2	n-$C_{10}H_{22} = 2 \cdot C_5H_{11}$	$7.85 \cdot 10^{14}$	0	34,146			
3	n-$C_{10}H_{22} = C_6H_{13} + nC_4H_9$	$1.05 \cdot 10^{15}$	0	34,146			
4	n-$C_{10}H_{22} = 1C_{10}H_{21} + H$	$8 \cdot 10^{14}$	0	50,998			
5	n-$C_{10}H_{22} = 2C_{10}H_{21} + H$	$8 \cdot 10^{14}$	0	50,998			
6	n-$C_{10}H_{22} = 3C_{10}H_{21} + H$	$8 \cdot 10^{14}$	0	50,998			
7	n-$C_{10}H_{22} = 4C_{10}H_{21} + H$	$8 \cdot 10^{14}$	0	50,998			
8	n-$C_{10}H_{22} = 5C_{10}H_{21} + H$	$8 \cdot 10^{14}$	0	50,998			
9	n-$C_{10}H_{22} + H = 1C_{10}H_{21} + H_2$	$4.7 \cdot 10^7$	2	3873			
10	n-$C_{10}H_{22} + H = 2C_{10}H_{21} + H_2$	$1.5 \cdot 10^7$	2	2516			
11	n-$C_{10}H_{22} + H = 3C_{10}H_{21} + H_2$	$1.5 \cdot 10^7$	2	2516			
12	n-$C_{10}H_{22} + H = 4C_{10}H_{21} + H_2$	$1.5 \cdot 10^7$	2	2516			
13	n-$C_{10}H_{22} + H = 5C_{10}H_{21} + H_2$	$1.5 \cdot 10^7$	2	2516			
14	n-$C_{10}H_{22} + OH = 1C_{10}H_{21} + H_2O$	$4.4 \cdot 10^9$	0.97	800			
15	n-$C_{10}H_{22} + OH = 2C_{10}H_{21} + H_2O$	$1.96 \cdot 10^7$	1.61	0			
16	n-$C_{10}H_{22} + OH = 3C_{10}H_{21} + H_2O$	$1.96 \cdot 10^7$	1.61	0			
17	n-$C_{10}H_{22} + OH = 4C_{10}H_{21} + H_2O$	$1.96 \cdot 10^7$	1.61	0	—	—	—
18	n-$C_{10}H_{22} + OH = 5C_{10}H_{21} + H_2O$	$1.96 \cdot 10^7$	1.61	0			
19	n-$C_{10}H_{22} + O = 1C_{10}H_{21} + OH$	$1.92 \cdot 10^6$	2.4	800			
20	n-$C_{10}H_{22} + O = 2C_{10}H_{21} + OH$	$5.33 \cdot 10^5$	2.5	2516			
21	n-$C_{10}H_{22} + O = 3C_{10}H_{21} + OH$	$5.33 \cdot 10^5$	2.5	2516			
22	n-$C_{10}H_{22} + O = 4C_{10}H_{21} + OH$	$5.33 \cdot 10^5$	2.5	2516			
23	n-$C_{10}H_{22} + O = 5C_{10}H_{21} + OH$	$5.33 \cdot 10^5$	2.5	2516			
24	n-$C_{10}H_{22} + CH_3 = 1C_{10}H_{21} + CH_4$	$2.5 \cdot 10^{12}$	0	5837			
25	n-$C_{10}H_{22} + CH_3 = 2C_{10}H_{21} + CH_4$	$1.33 \cdot 10^{12}$	0	4781			
26	n-$C_{10}H_{22} + CH_3 = 3C_{10}H_{21} + CH_4$	$1.33 \cdot 10^{12}$	0	4781			
27	n-$C_{10}H_{22} + CH_3 = 4C_{10}H_{21} + CH_4$	$1.33 \cdot 10^{12}$	0	4781			
28	n-$C_{10}H_{22} + CH_3 = 5C_{10}H_{21} + CH_4$	$1.33 \cdot 10^{12}$	0	4781			
29	n-$C_{10}H_{22} + HO_2 = 1C_{10}H_{21} + H_2O_2$	$9.33 \cdot 10^{12}$	0	9763			
30	n-$C_{10}H_{22} + HO_2 = 2C_{10}H_{21} + H_2O_2$	$5.67 \cdot 10^{12}$	0	8555			
31	n-$C_{10}H_{22} + HO_2 = 3C_{10}H_{21} + H_2O_2$	$5.67 \cdot 10^{12}$	0	8555			
32	n-$C_{10}H_{22} + HO_2 = 4C_{10}H_{21} + H_2O_2$	$5.67 \cdot 10^{12}$	0	8555			
33	n-$C_{10}H_{22} + HO_2 = 5C_{10}H_{21} + H_2O_2$	$5.67 \cdot 10^{12}$	0	8555			

TABLE 1 (Continued)

No.	Reaction	k_{+q}			k_{-q}		
		A_q, cm, mole, sec	n_q	E_{aq}, K	A_q, cm, mole, sec	n_q	E_{aq}, K
34	n-$C_{10}H_{22} + O_2 = 1C_{10}H_{21} + HO_2$	$2.09 \cdot 10^{13}$	0	26,235			
35	n-$C_{10}H_{22} + O_2 = 2C_{10}H_{21} + HO_2$	$3.3 \cdot 10^{13}$	0	24,537			
36	n-$C_{10}H_{22} + O_2 = 3C_{10}H_{21} + HO_2$	$3.3 \cdot 10^{13}$	0	24,537			
37	n-$C_{10}H_{22} + O_2 = 4C_{10}H_{21} + HO_2$	$3.3 \cdot 10^{13}$	0	24,537			
38	n-$C_{10}H_{22} + O_2 = 5C_{10}H_{21} + HO_2$	$3.3 \cdot 10^{13}$	0	24,537			
39	$1C_{10}H_{21} = 1C_8H_{17} + C_2H_4$	$2.1 \cdot 10^{13}$	0	14,554			
40	$2C_{10}H_{21} = C_7H_{15} + C_3H_6$	$2.1 \cdot 10^{13}$	0	13,231			
41	$3C_{10}H_{21} = C_6H_{13} + C_4H_8$	$2.1 \cdot 10^{13}$	0	13,231			
42	$4C_{10}H_{21} = C_5H_{11} + C_5H_{10}$	$2.1 \cdot 10^{13}$	0	12,870			
43	$4C_{10}H_{21} = C_8H_{16} + C_2H_5$	$1 \cdot 10^{13}$	0	14,554	—	—	—
44	$5C_{10}H_{21} = C_6H_{12} + nC_4H_9$	$4.2 \cdot 10^{13}$	0	12,990			
45	$5C_{10}H_{21} = C_7H_{14} + nC_3H_7$	$2.1 \cdot 10^{13}$	0	14,554			
46	$1C_{10}H_{21} = 4C_{10}H_{21}$	$2 \cdot 10^{11}$	0	10,103			
47	$1C_{10}H_{21} = 5C_{10}H_{21}$	$2 \cdot 10^{11}$	0	10,103			
48	$2C_{10}H_{21} = 4C_{10}H_{21}$	$2 \cdot 10^{11}$	0	10,103			
49	$2C_{10}H_{21} = 5C_{10}H_{21}$	$2 \cdot 10^{11}$	0	10,103			
50	$3C_{10}H_{21} = 4C_{10}H_{21}$	$2 \cdot 10^{11}$	0	10,103			
51	$3C_{10}H_{21} = 5C_{10}H_{21}$	$2 \cdot 10^{11}$	0	10,103			
52	$1C_{10}H_{21} = C_{10}H_{20} + H$	$4.2 \cdot 10^{16}$	-0.94	19,000	$1 \cdot 10^{13}$	0	1260
53	$2C_{10}H_{21} = C_{10}H_{20} + H$	$4.2 \cdot 10^{16}$	-0.94	19,000	$1 \cdot 10^{13}$	0	1260
54	$3C_{10}H_{21} = C_{10}H_{20} + H$	$4.2 \cdot 10^{16}$	-0.94	19,000	$1 \cdot 10^{13}$	0	1260
55	$4C_{10}H_{21} = C_{10}H_{20} + H$	$4.2 \cdot 10^{16}$	-0.94	19,000	$1 \cdot 10^{13}$	0	1260
56	$5C_{10}H_{21} = C_{10}H_{20} + H$	$4.2 \cdot 10^{16}$	-0.94	19,000	$1 \cdot 10^{13}$	0	1260
57	$1C_{10}H_{21} + O_2 = C_{10}H_{20} + HO_2$	$1 \cdot 10^{10}$	0	5000	$1 \cdot 10^{11}$	0	10,000
58	$2C_{10}H_{21} + O_2 = C_{10}H_{20} + HO_2$	$1 \cdot 10^{10}$	0	5000	$1 \cdot 10^{11}$	0	10,000
59	$3C_{10}H_{21} + O_2 = C_{10}H_{20} + HO_2$	$1 \cdot 10^{10}$	0	5000	$1 \cdot 10^{11}$	0	10,000
60	$4C_{10}H_{21} + O_2 = C_{10}H_{20} + HO_2$	$1 \cdot 10^{10}$	0	5000	$1 \cdot 10^{11}$	0	10,000
61	$5C_{10}H_{21} + O_2 = C_{10}H_{20} + HO_2$	$1 \cdot 10^{10}$	0	5000	$1 \cdot 10^{11}$	0	10,000
62	$C_{10}H_{20} = C_7H_{15} + C_3H_5$	$3.5 \cdot 10^{16}$	0	35,723	0	0	0
63	$C_{10}H_{20} = nC_4H_9 + C_6H_{11}$	$3.5 \cdot 10^{16}$	0	35,723	0	0	0
64	$C_{10}H_{20} = C_5H_{11} + C_5H_9$	$3.5 \cdot 10^{16}$	0	35,723	0	0	0
65	$C_{10}H_{20} = C_2H_5 + C_8H_{15}$	$3.5 \cdot 10^{16}$	0	35,723	0	0	0
66	$C_{10}H_{20} = 1C_8H_{17} + C_2H_3$	$3.5 \cdot 10^{16}$	0	35,723	0	0	0

TABLE 1 (Continued)

No.	Reaction	k_{+q}			k_{-q}		
		A_q, cm, mole, sec	n_q	E_{aq}, K	A_q, cm, mole, sec	n_q	E_{aq}, K
67	$C_{10}H_{20} + OH = CH_3CHO + 1C_8H_{17}$	$1 \cdot 10^{11}$	0	−2020	0	0	0
68	$C_{10}H_{20} + OH = C_4H_8O + C_6H_{13}$	$1 \cdot 10^{11}$	0	−2020	0	0	0
69	$C_{10}H_{20} + OH = C_3H_6O + C_7H_{15}$	$1 \cdot 10^{11}$	0	−2020	0	0	0
70	$C_{10}H_{20} + O = CH_3CHO + C_8H_{16}$	$1 \cdot 10^{11}$	0	−530	0	0	0
71	$C_{10}H_{20} + O = CH_2CHO + 1C_8H_{17}$	$1 \cdot 10^{11}$	0	−530	0	0	0
72	$C_{10}H_{20} + O = C_3H_5O + C_7H_{15}$	$1 \cdot 10^{11}$	0	−530	0	0	0
73	$C_{10}H_{20} + O = C_4H_8O + C_6H_{12}$	$1 \cdot 10^{11}$	0	−530	0	0	0
74	$1C_{10}H_{21} + O_2 = C_{10}H_{21}O_2$	$7.54 \cdot 10^{12}$	0	0	$1.05 \cdot 10^{23}$	−2.32	19,600
75	$2C_{10}H_{21} + O_2 = C_{10}H_{21}O_2$	$7.54 \cdot 10^{12}$	0	0	$1.05 \cdot 10^{23}$	−2.32	19,600
76	$3C_{10}H_{21} + O_2 = C_{10}H_{21}O_2$	$7.54 \cdot 10^{12}$	0	0	$1.05 \cdot 10^{23}$	−2.32	19,600
77	$4C_{10}H_{21} + O_2 = C_{10}H_{21}O_2$	$7.54 \cdot 10^{12}$	0	0	$1.05 \cdot 10^{23}$	−2.32	19,600
78	$5C_{10}H_{21} + O_2 = C_{10}H_{21}O_2$	$7.54 \cdot 10^{12}$	0	0	$1.05 \cdot 10^{23}$	−2.32	19,600
79	$C_{10}H_{21}O_2 = C_{10}H_{20}OOH$	$2 \cdot 10^{11}$	0	8564	$1 \cdot 10^{11}$	0	6290
80	$C_{10}H_{20}OOH = C_{10}H_{20} + HO_2$	$8.5 \cdot 10^{12}$	0	12,870	0	0	0
81	$C_{10}H_{20}OOH + O_2 = OOC_{10}H_{20}OOH$	$5 \cdot 10^{11}$	0	0	0	0	0
82	$OOC_{10}H_{20}OOH = OC_{10}H_{19}OOH + OH$	$1.5 \cdot 10^{14}$	0	12,509	0	0	0
83	$OC_{10}H_{19}OOH = CH_3CO_3 + 4C_8H_{17}$	$7 \cdot 10^{15}$	0	21,169	0	0	0
84	$C_{10}H_{21}O_2 + HO_2 = C_{10}H_{21}OOH + O_2$	$1 \cdot 10^{11}$	0	0	$3 \cdot 10^{11}$	0	19,700
85	$C_{10}H_{21}O_2 + H_2O_2 = C_{10}H_{21}OOH + HO_2$	$2.4 \cdot 10^{12}$	0	5050	$2.4 \cdot 10^{12}$	0	5050
86	$C_{10}H_{21}O_2 + n\text{-}C_{10}H_{22} = C_{10}H_{21}OOH + 1C_{10}H_{21}$	$1.21 \cdot 10^{13}$	0	10,300	$1.44 \cdot 10^{10}$	0	7580
87	$C_{10}H_{21}O_2 + n\text{-}C_{10}H_{22} = C_{10}H_{21}OOH + 2C_{10}H_{21}$	$1.21 \cdot 10^{13}$	0	10,300	$1.44 \cdot 10^{10}$	0	7580
88	$C_{10}H_{21}O_2 + n\text{-}C_{10}H_{22} = C_{10}H_{21}OOH + 3C_{10}H_{21}$	$1.21 \cdot 10^{13}$	0	10,300	$1.44 \cdot 10^{10}$	0	7580
89	$C_{10}H_{21}O_2 + n\text{-}C_{10}H_{22} = C_{10}H_{21}OOH + 4C_{10}H_{21}$	$1.21 \cdot 10^{13}$	0	10,300	$1.44 \cdot 10^{10}$	0	7580
90	$C_{10}H_{21}O_2 + n\text{-}C_{10}H_{22} = C_{10}H_{21}OOH + 5C_{10}H_{21}$	$1.21 \cdot 10^{13}$	0	10,300	$1.44 \cdot 10^{10}$	0	7580
91	$C_{10}H_{21}O_2 + CH_3O_2 = C_{10}H_{21}O + CH_3O + O_2$	$1 \cdot 10^{11}$	0	0	0	0	0
92	$C_{10}H_{21}O_2 + 1C_{10}H_{21} = 2 \cdot C_{10}H_{21}O$	$1.9 \cdot 10^{12}$	0	−606	$1 \cdot 10^{10}$	0	0
93	$C_{10}H_{21}O_2 + 2C_{10}H_{21} = 2 \cdot C_{10}H_{21}O$	$1.9 \cdot 10^{12}$	0	−606	$1 \cdot 10^{10}$	0	0
94	$C_{10}H_{21}O_2 + 3C_{10}H_{21} = 2 \cdot C_{10}H_{21}O$	$1.9 \cdot 10^{12}$	0	−606	$1 \cdot 10^{10}$	0	0
95	$C_{10}H_{21}O_2 + 4C_{10}H_{21} = 2 \cdot C_{10}H_{21}O$	$1.9 \cdot 10^{12}$	0	−606	$1 \cdot 10^{10}$	0	0
96	$C_{10}H_{21}O_2 + 5C_{10}H_{21} = 2 \cdot C_{10}H_{21}O$	$1.9 \cdot 10^{12}$	0	−606	$1 \cdot 10^{10}$	0	0
97	$2 \cdot C_{10}H_{21}O_2 = 2 \cdot C_{10}H_{21}O + O_2$	$1 \cdot 10^{11}$	0	0	0	0	0
98	$C_{10}H_{21}OOH = C_{10}H_{21}O + OH$	$2.9 \cdot 10^{20}$	−1.71	23,400	$1 \cdot 10^{13}$	0	0

TABLE 1 (Final)

No.	Reaction	k_{+q}			k_{-q}		
		A_q, cm, mole, sec	n_q	E_{aq}, K	A_q, cm, mole, sec	n_q	E_{aq}, K
99	$C_{10}H_{20}OOH = C_{10}H_{20}O + OH$	$3 \cdot 10^{11}$	0	11,100	0	0	0
100	$C_{10}H_{21}O = C_7H_{15} + C_2H_4 + CH_2O$	$2 \cdot 10^{13}$	0	7580	0	0	0
101	$C_{10}H_{20}O + OH = C_8H_{16} + CH_3CO + H_2O$	$4.42 \cdot 10^9$	1	−75.2	0	0	0
102	$C_{10}H_{20}O + OH = 1C_8H_{17} + CH_2CO + H_2O$	$4.42 \cdot 10^9$	1	−75.2	0	0	0
103	$C_{10}H_{20}O + OH = 2C_8H_{17} + CH_2CO + H_2O$	$4.42 \cdot 10^9$	1	−75.2	0	0	0
104	$C_{10}H_{20}O + OH = 3C_8H_{17} + CH_2CO + H_2O$	$4.42 \cdot 10^9$	1	−75.2	0	0	0
105	$C_{10}H_{20}O + OH = 4C_8H_{17} + CH_2CO + H_2O$	$4.42 \cdot 10^9$	1	−75.2	0	0	0
106	$C_{10}H_{20}O + OH = C_7H_{14} + C_3H_5O + H_2O$	$8.84 \cdot 10^9$	1	−75.2	0	0	0
107	$C_{10}H_{20}O + OH = C_8H_{15} + CH_3CHO + H_2O$	$2.34 \cdot 10^7$	1.61	−17.7	0	0	0
108	$C_{10}H_{20}O + HO_2 = C_8H_{16} + CH_2CHO + H_2O_2$	$6 \cdot 10^4$	2.6	7030	0	0	0
109	$C_{10}H_{20}O + HO_2 = C_8H_{16} + CH_3CO + H_2O_2$	$1.08 \cdot 10^4$	2.55	5320	0	0	0
110	$C_{10}H_{20}O + HO_2 = C_7H_{14} + C_3H_5O + H_2O_2$	$2.16 \cdot 10^4$	2.55	5320	0	0	0
111	$C_{10}H_{20}O + HO_2 = 1C_8H_{17} + CH_2CO + H_2O_2$	$1.08 \cdot 10^4$	2.55	5320	0	0	0
112	$C_{10}H_{20}O + HO_2 = C_8H_{15} + CH_3CHO + H_2O_2$	$1.48 \cdot 10^4$	2.6	7030	0	0	0
113	$C_{10}H_{20}O + HO_2 = C_7H_{13} + C_3H_6O + H_2O_2$	$1.48 \cdot 10^4$	2.6	7030	0	0	0

Hydroperoxide ROOH can dissociate with formation of two active radicals: RO and OH (class 19). Thus, the reaction $RO_2 + H_2O_2 = ROOH + HO_2$ leads to branching of the chain mechanism and accelerates ignition at low temperatures.

The radicals RO and also QO formed as a result of splitting of the O—O bond in the hydroperoxide QOOH (class 15) dissociate and interact with OH and HO_2 radicals (classes 16 and 22) with formation of lower hydrocarbons.

It should be noted that this kinetic mechanism owing to its modular structure can be easily extended to describe oxidation and ignition of heavier alkanes n-$C_{12}H_{26}$, n-$C_{14}H_{30}$, and n-$C_{16}H_{34}$.

COMPARISONS WITH EXPERIMENTAL DATA

To determine whether the proposed kinetic mechanism is able to provide a correct and accurate description of ignition of the n-$C_{10}H_{22}$/air mixture in wide ranges of temperatures, pressures, and mixture compositions, we performed comparisons with experimental data obtained behind the shock wave reflected from the end face of the tunnel by the shock-tube technique [22–29] and with concentration profiles of various species measured in a flow reactor [30]. Note that ignition and pyrolysis under these experimental conditions are controlled only by kinetics, and the transport process exerts no effect on the measured quantities as it happens, for instance, in diffusion flames. Comparisons with the ignition delay times calculated with the use of other reaction mechanisms are also discussed in the paper. To avoid errors and inaccuracies in reproducing these calculations, comparisons with experimental data are always performed with modeling results obtained by the authors of the reaction mechanisms.

The ignition delay time (otherwise called the induction time) τ_{ind} was measured for both n-$C_{10}H_{22}/O_2/Ar$ and n-$C_{10}H_{22}/O_2/N_2$ mixtures in wide ranges of initial pressures (p_0 = 1–80 atm), temperatures (T_0 = 650–1640 K), and compositions of the mixture (fuel-to-air equivalence ratio ϕ = 0.5–3). In the case of shock wave reflection from a flat end face, the gas density behind the reflected shock wave is known to be constant in most cases, and ignition of the combustible mixture in a closed adiabatic reactor can be modeled by using a zero-dimensional approximation for an ideal inviscid heat-non-conducting gas in a closed adiabatic reactor. Translational, rotational, and vibrational degrees of freedom of molecules are assumed to be in thermodynamic equi-

librium. The system of governing equations for such a system includes equations that describe the changes in the gas temperature and species concentrations, as well as the equation of state [50]. The initial conditions for this system of equations are the gas temperature and pressure, as well as the composition of the mixture at the time instant $t = 0$.

It should be noted that most shock-tube experiments on determining the ignition delay time were performed at rather high temperatures ($T_0 > 1200$ K) behind the reflected shock wave front [22–24, 26, 29]. There are only few experimental works where the results were obtained both at low ($T_0 < 1000$ K) and high temperatures [27, 28]. Even high-temperature oxidation of *n*-decane is described well only by detailed and lumped models. Figure 2 shows the dependences $\tau_{\text{ind}}(T_0)$ obtained by using the models developed in [12] and [30], and the model of this work, as well as the experimental data [23] for a stoichiometric $C_{10}H_{22}/O_2$ mixture diluted by argon at $p_0 = 1.2$–1.3 atm. It is seen that the reaction mechanism [30] including 449 reversible reactions and 58 species (it can be considered as a skeleton mechanism) and built for describing high-temperature ignition of *n*-decane only does not ensure reasonable agreement with the experimental data (systematic overprediction of τ_{ind} by a factor of 8 to 10 is observed). At the same time, the results calculated by the reaction mechanism developed in [12] and including 1483 reversible reactions with participation of 210 chemical species and by the present model agree well with the measurements. Both these mechanisms are lumped ones. In contrast to the present kinetic model, however, the model developed in [12] does not include the low-temperature oxidation mechanism [the model developed in [12] still slightly underpredicts the measured values of τ_{ind} (by 20–30%)]. This fact testifies that skeleton mechanisms do not ensure an accurate description of experimental data even in the high-temperature region, whereas lumped and detailed mechanisms allow this to be done.

Fairly accurate measurements of the ignition delay time in a wide range of compositions of the n-$C_{10}H_{22}/O_2/Ar$ mixture ($\phi = 0.57$–3) in the temperature interval $T_0 = 1237$–1616 K at moderate pressures $p_0 = 1.8$–10 atm were recently performed in [22] with moderate heating of the shock-tube walls. To describe their experiments, Olchanski and Burcat [22] proposed a kinetic model including 433 reactions and 69 chemical species (this model does not contain the low-temperature mechanism). Note that this model is based on earlier publications of other researchers from which the basic reactions responsible for the chain process development with the corresponding rate constants of forward reactions were borrowed, and the rate constants of backward reactions were calculated on the basis of the principle of detailed equilibrium balancing. Thermodynamic properties of heavy hydrocarbons were refined by Olchanski and Burcat [22]. All experimental data obtained in [22] were generalized by a dependence including the concentrations of individual species of the mixture and the measured ignition delay times (induction times): $\beta = \tau_{\text{ind}}/([C_{10}H_{22}]^{0.6}[O_2]^{-1.305}[Ar]^{0.08})$. Figure 3 shows the experimental data [22] and the results calculated by the model proposed in [22] with the use of the reaction mechanism [31] and by the present model. It is seen that the reaction mechanism proposed in [31] does not ensure good agreement with the experimental data. At the same time, the present model, as well as the model developed in [22], offers a good description of the experimental data.

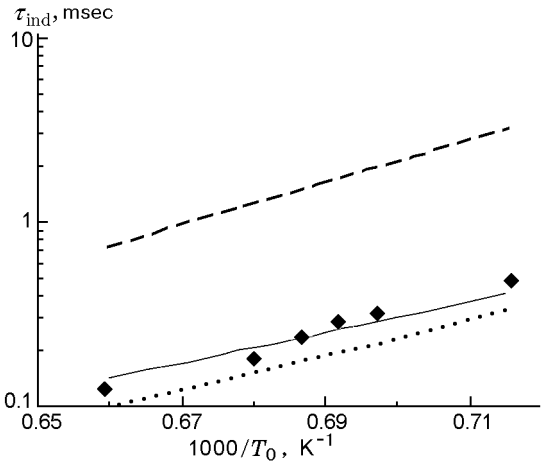

Fig. 2. Ignition delay time in a (0.2% n-$C_{10}H_{22}$)/(3.1% O_2/Ar) mixture at $\phi = 1$ and $p_0 = 1.2$–1.3 atm: the points are the experimental data [23]; the dotted and dashed curves are the results calculated by the models developed in [30] and [12], respectively; the solid curve shows the calculation by the mechanism proposed in the present work.

For various applications, it is necessary to ensure not only a correct description of oxidation kinetics at high temperatures ($T > 1000$ K), but also accurate calculations of the ignition characteristics at low temperatures ($T = 650$–1000 K). In this range of temperatures, one can also observe cold-flame phenomena associated with formation of an ignition precursor, where the gas temperature increases, but the mixture is not ignited, though ignition can occur at later stages of the process. The values of τ_{ind} at $T_0 = 650$–1300 K for the n-$C_{10}H_{22}$/air mixture at $\phi = 1$ and 2, $p_0 = 13$ and 50 atm were measured in [27, 28]. Figure 4 shows the ex-

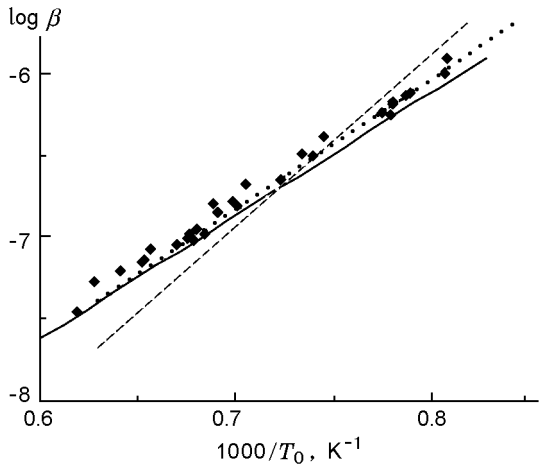

Fig. 3. Behavior of the parameter β as a function of temperature for the n-$C_{10}H_{22}/O_2/Ar$ mixture: the points are the experimental data [22]; the dashed, dotted, and solid curves show the results calculated by the models developed in [31], [22], and in this paper, respectively.

perimental data [27, 28] and the values of τ_{ind} calculated by the present model and by the model developed in [32], which includes ≈600 reactions with 67 species and contains the low-temperature mechanism of n-decane oxidation. At low temperatures T_0 = 650–750 K and p_0 = 50 atm, the kinetic model [32] substantially overpredicts the values of τ_{ind} (by a factor of 3–5) as compared with the experiment, both for the stoichiometric (ϕ = 1) and for the fuel-rich (ϕ = 2) mixtures. At lower pressures (p_0 = 13 atm) and the temperature T_0 = 800 K, that model, vice versa, underpredicts the values of τ_{ind} (the values are approximately twice lower than the experimental data). The present model ensures much better coincidence with experimental data (the difference between the calculated and measured values of τ_{ind} does not exceed 15%).

Moreover, the present model provides a correct description of the experimental results [27] with measurements of τ_{ind} for the fuel-lean n-$C_{10}H_{22}$/air mixture (ϕ = 0.5 and 0.67) as well. This fact is illustrated in Fig. 5, which shows the values of τ_{ind} measured in [27] and predicted by the present model. The values of τ_{ind} for the stoichiometric (ϕ = 1) and fuel-lean (ϕ = 0.5) n-$C_{10}H_{20}$/air mixtures were recently measured in [28] at higher pressures (p_0 = 80 atm) in a rather wide range of temperatures T_0 = 700–1350 K. Westbrook et al. [21] made an attempt to describe these results on the basis of a detailed reaction mechanism including 3878 reactions and 940 species. For comparison, Fig. 6 shows the experimental data [28] and the results calculated by the model [21] and by the present model. It is seen that the

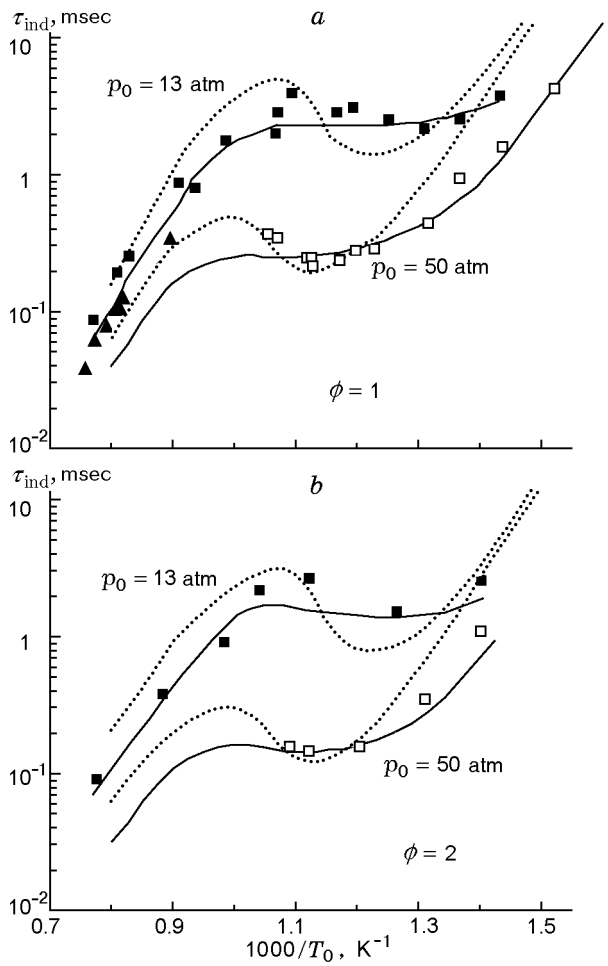

Fig. 4. Ignition delay time of the n-$C_{10}H_{22}$/air mixture at ϕ = 1 (a) and 2 (b): the points show the experimental results [27] at p_0 = 13 (■) and 50 atm (□) and the experimental results [28] at p_0 = 13 atm (▲); the dotted and solid curves show the data calculated by the model [32] and by the present model, respectively.

present model (which is simpler and can be classified as a lumped model) ensures substantially better agreement with the experiment (the error is within 25%) than the detailed reaction mechanism [21]. The values of τ_{ind} predicted by the mechanism [21] differ from the experimental results measured, for instance, at T_0 = 900 K and ϕ = 1 by a factor of 2.2. The same difference in the values of τ_{ind} is also observed for the fuel-lean mixture (ϕ = 0.5). Thus, we can state that the model developed in [21] systematically overpredicts the value of τ_{ind} in the low-temperature region (T < 1000 K). This means that introduction of various isomers of higher alkenes and isomers of their derivatives, as it was done in [21], does not necessarily improve the predictive capability of the kinetic model.

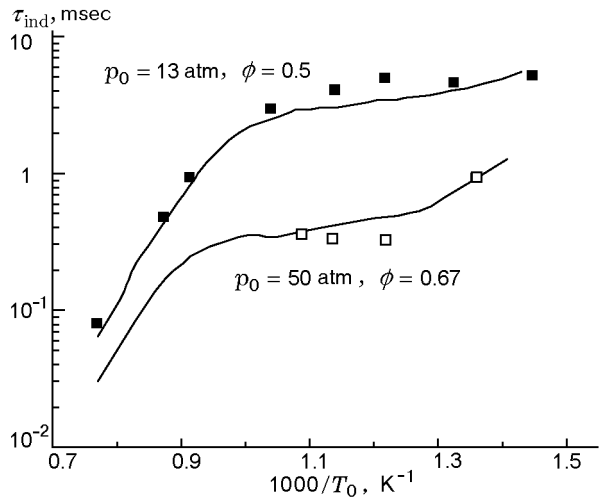

Fig. 5. Ignition delay time of the n-$C_{10}H_{22}$/air mixture at $\phi = 0.5$, $p_0 = 13$ atm and $\phi = 0.67$, $p_0 = 50$ atm: the points and curves are the experimental data [27] and the predictions of the present model.

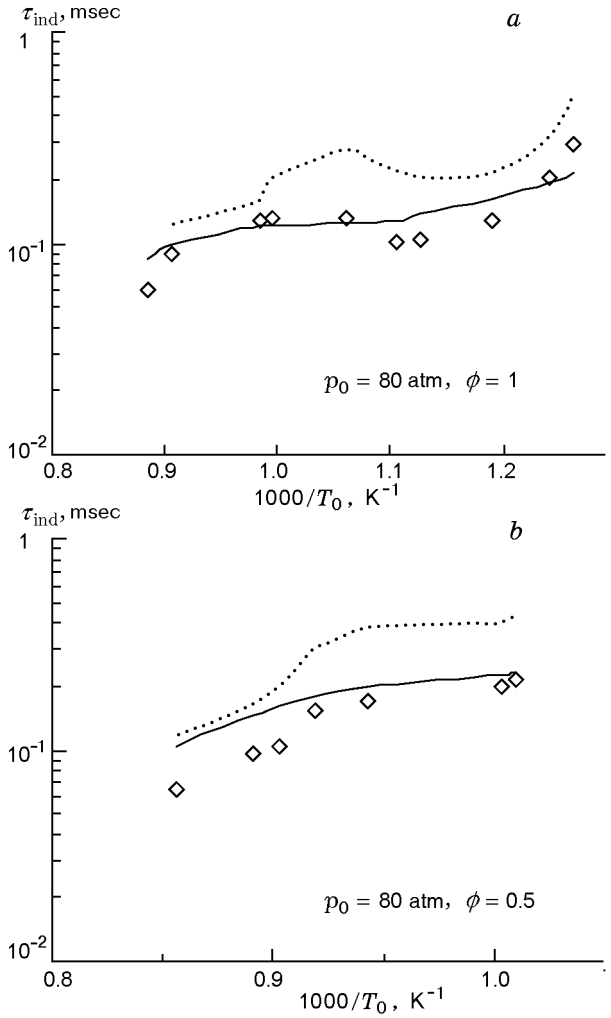

Fig. 6. Ignition delay time of the n-$C_{10}H_{22}$/air mixture at $\phi = 1$ and 0.5, $p_0 = 80$ atm: the points are the experimental data [28]; the dotted and solid curves show the results calculated by the model developed in [21] and by the present model, respectively.

It should be noted that both the kinetic model [32] and the later and more detailed model [21] in the temperature range $T_0 = 950$–750 K predict a much more intense decrease in τ_{ind} with decreasing temperature [the so-called negative temperature coefficient in the dependence $\tau_{ind}(T_0)$] than that registered in the experiment. The present model predicts a considerably smaller negative temperature coefficient in this range of T_0, and this feature become most noticeably apparent for fuel-rich ($\phi = 2$) mixtures (see Fig. 4b). For the stoichiometric ($\phi = 1$) mixture, both the present model and the experimental data [27, 28] give a weaker negative temperature coefficient. The negative temperature coefficient is almost absent for the fuel-lean mixture ($\phi = 0.5$) (the growth of τ_{ind} with decreasing T_0 is only slowed down in the interval $T_0 = 950$–750 K). Note that this behavior of the dependence $\tau_{ind}(T_0)$ is typical for all heavy alkanes beginning from n-C_7H_{16} and is most revealed for the n-C_7H_{16}/air mixture [7–9, 21]. The fact that the negative temperature coefficient for n-decane is smaller than that for n-heptane can be attributed to the less important role of the reaction of H atom abstraction from alkene C_nH_{2n} at $T < 1200$ K for saturated hydrocarbons C_nH_{2n+2} with increasing n. This hypothesis, however, needs both experimental and theoretical justification.

Dean et al. [29] performed precision measurements of τ_{ind} in the n-decane–air mixture on the basis of several parameters behind the reflected shock wave in the range $T_0 = 1100$–1800 K at $p_0 = 8.9$ atm. The results of these measurements correlate well with the experimental data [27] obtained at a slightly higher pressure ($p_0 = 13$ atm). It is well seen from Fig. 7. Comparing the values of τ_{ind} calculated by this kinetic model with those measured in [27, 29], we can conclude that the model proposed in the present work accurately describes the experimental data for pressures $p_0 = 8.9$–13 atm as well. It also follows from the results presented in Fig. 7 that the ignition delay time changes insignificantly as the pressure of the mixture is varied from 8.9 to 13 atm.

The ignition delay time (otherwise called the induction time) is actually an integral characteristic of ignition determining the rate of chain process development. The theoretical analysis of n-decane oxidation mechanisms under various conditions requires the use of a kinetic model capable of accurate reproduc-

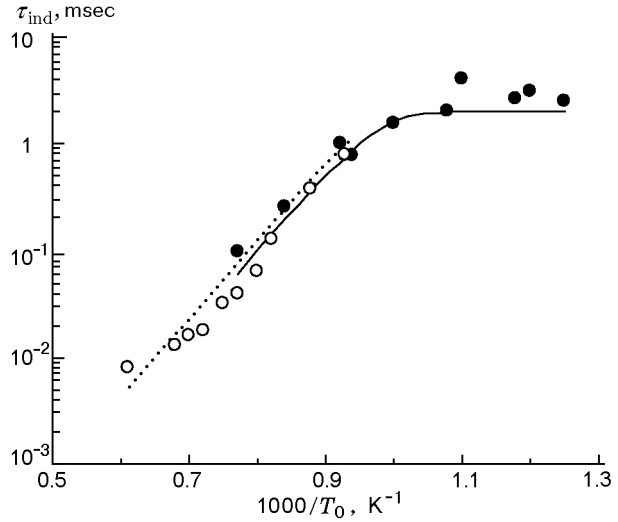

Fig. 7. Ignition delay time of the n-$C_{10}H_{22}$/air mixture at $\phi = 1$: the points show the experimental results [27] at $p_0 = 13$ atm (●) and [29] at $p_0 = 8.9$ atm (○); the solid and dotted curves are the calculations by the present model at $p_0 = 13$ and 8.9 atm, respectively.

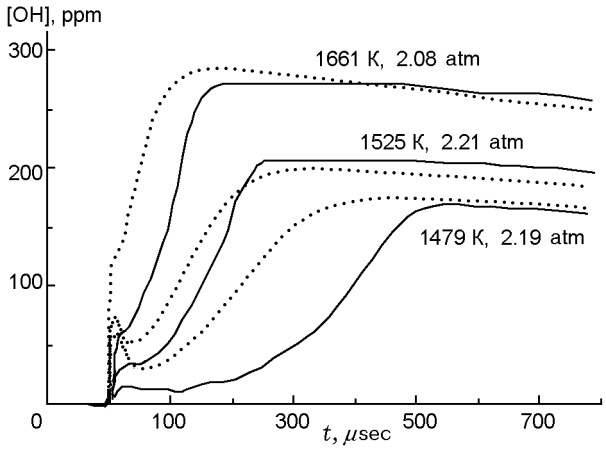

Fig. 8. Evolution of the mole fraction of the OH radical behind the reflected shock wave front for the stoichiometric n-$C_{10}H_{22}/O_2/Ar$ mixture (300 ppm n-$C_{10}H_{22}$) for different values of temperature and pressure: the solid and dotted curves show the experimental data [26] and the results calculated by the present model.

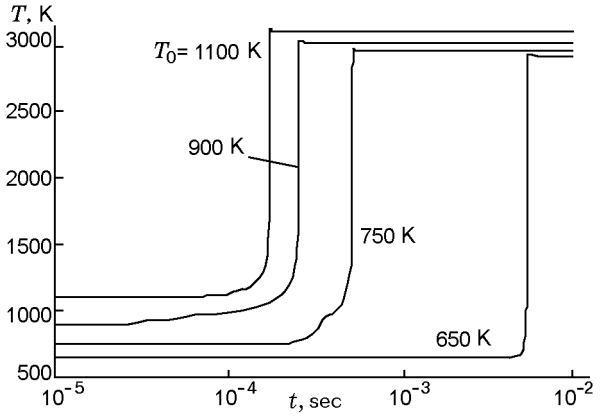

Fig. 9. Time history of temperature during ignition of the stoichiometric n-$C_{10}H_{22}$/air mixture in an adiabatic reactor at $p_0 = 50$ atm and $T_0 = 1100$, 900, 750, and 650 K.

tion of the behavior of active radicals OH, CH_3, CH_2O, C_3H_5, etc., and O and H atoms, which are carriers of the chain process in hydrocarbon–air mixtures. Therefore, during verification of the kinetic model, it is also desirable to use experimental data on concentrations of such active species in the ignition process. Davidson et al. [26] performed such measurements for the OH radical behind the front of the reflected shock wave in the n-$C_{10}H_{22}/O_2/Ar$ mixture at different values of T_0. In Fig. 8, the measured OH concentrations are compared with the values calculated by the model of the present work at $T_0 = 1479$, 1525, and 1661 K and at $p_0 = 2.19$, 2.21, and 2.08 atm, respectively. It is seen that the model ensures an accurate description of the experimental data [26]; it is only at $T_0 = 1479$ K that the calculations predict a faster change in the OH concentration than that observed in the experiment. It should be noted that both the calculated and experimental data display a local maximum on the time profile of the OH concentration behind the shock wave front for all conditions considered.

Thus, we can conclude that the proposed lumped reaction mechanism provides a satisfactory description of available experimental data on ignition of n-decane mixed with O_2 or with air in both the high-temperature ($T_0 > 1000$ K) and low-temperature ($T_0 < 1000$ K) ranges.

As was noted above, the mechanisms responsible for ignition of the n-$C_{10}H_{22}/O_2$(air) mixture at comparatively low temperatures ($T_0 = 950$–750 K) have not been completely clarified for many hydrocarbons, including n-decane. Cold-flame phenomena have not been explained either. To discuss the latter, let us consider the time history of the temperature of the mixture and the concentrations of the basic species, carriers of the chain mechanism, for different values of T_0. The distributions $T(t)$ for the stoichiometric n-$C_{10}H_{22}$/air mixture with $p_0 = 50$ atm at $T_0 = 650$, 750, 900, and 1100 K are shown in Fig. 9. It is seen that the dependences $T(t)$ at $T_0 = 750$ and 900 K are noticeably different from these dependences at $T_0 = 1100$ and 650 K. An increase in temperature occurs before igni-

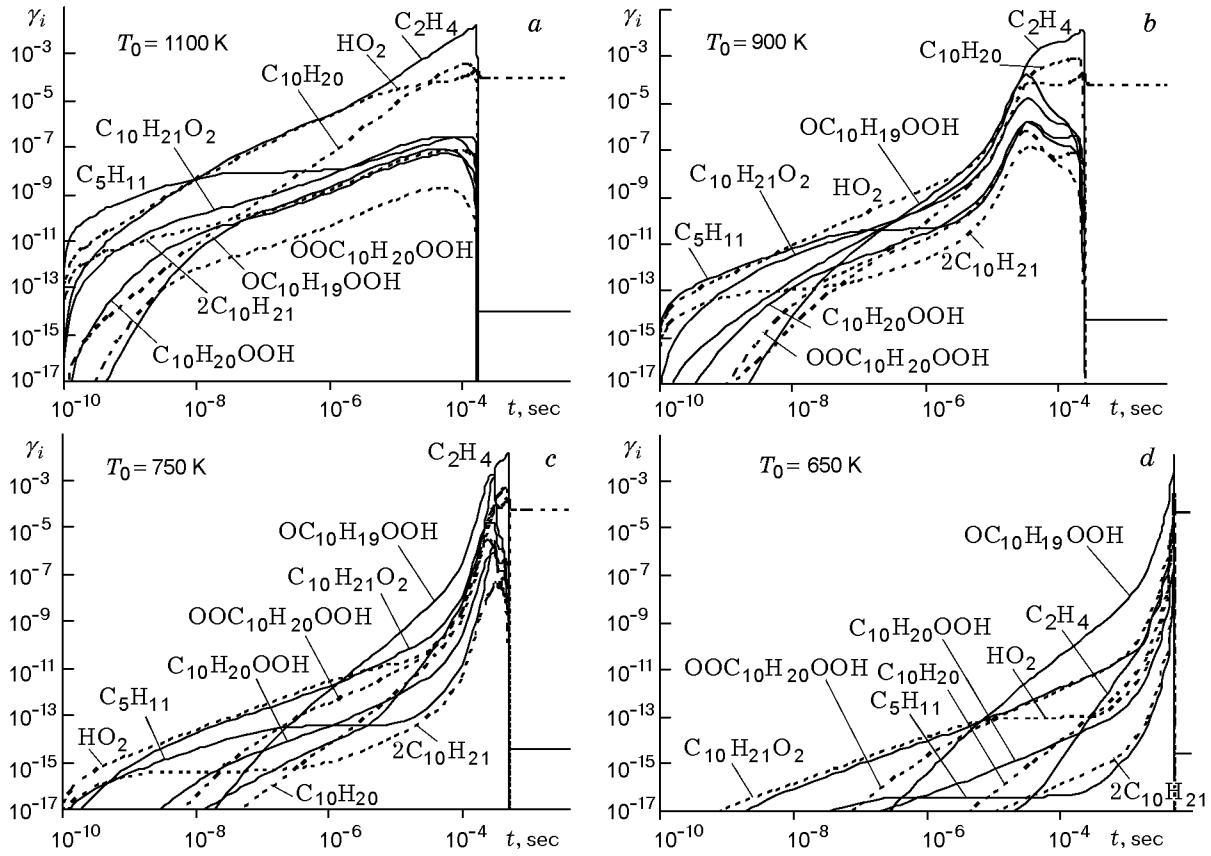

Fig. 10. Time history of the mole fractions γ_i of the basic species in the case of ignition of the stoichiometric n-$C_{10}H_{22}$/air mixture in an adiabatic reactor at $p_0 = 50$ atm and $T_0 = 1100$ (a), 900 (b), 750 (c), and 650 K (d).

tion of the mixture in the interval $T_0 = 1000$–750 K, i.e., cold-flame phenomena are obviously observed. Another interesting fact is a drastic increase in the induction time as the temperature T_0 decreases from 750 to 650 K. The change in the behavior of the dependence $T(t)$ with the initial temperature decreasing from 1100 to 900 K is caused by the change in the chain mechanism of n-decane oxidation with decreasing T_0. Figure 10 shows the behavior of the mole fractions γ_i of the basic species responsible for ignition of the n-$C_{10}H_{22}$/air mixture at $T_0 = 1100$, 900, 750, and 650 K in an adiabatic reactor. As the concentrations of different alkyl radicals C_nH_{2n+1} evolve in time in a similar manner, Fig. 10 shows only the curves for the C_5H_{11} mole fraction, which has the maximum concentration, and for the $2C_{10}H_{21}$ radical. The group of alkenes C_nH_{2n} is presented by ethylene C_2H_4 and $C_{10}H_{20}$. It is seen in Fig. 10 that different species formed during n-decane oxidation dominate in the interval $[0; \tau_{\text{ind}}]$, depending on T_0.

At a higher initial temperature ($T_0 = 1100$ K), alkyl radicals C_5H_{11}, C_6H_{13}, C_7H_{15}, n-C_4H_9, and n-C_3H_7 are mainly formed at the initial stage of the oxidation process $0 < t \leqslant 10^{-8}$ sec. The processes of monomolecular decomposition (reaction Nos. 1–3) are responsible for the emergence of these radicals. Hereinafter, the numeration of reactions corresponds to the numeration in Table 1. The rate of formation of $kC_{10}H_{21}$ ($k = 1, \ldots, 5$) radicals through dissociation of n-$C_{10}H_{22}$ (reaction Nos. 4–8) at $T_0 = 1100$ K is slightly lower because of the higher activation energy barrier of this process. The $kC_{10}H_{21}$ radicals form more actively during interaction of n-$C_{10}H_{22}$ with oxygen (reaction Nos. 34–38). At $t > 10^{-8}$ sec, the highest concentrations are observed for HO_2 and olefins C_2H_4, C_3H_6, C_4H_8, C_6H_{12}, C_7H_{14}, and $C_{10}H_{20}$, which are formed through interaction of alkyl radicals with O_2 (reaction Nos. 57–61). These species prevail in the mixture before the ignition event $t = 1.7 \cdot 10^{-4}$ sec. These reactions are typical for the high-temperature oxidation mecha-

nism. At the temperature $T_0 = 1100$ K, the formation of alkylperoxide $C_{10}H_{21}O_2$ (reactions 74–78) is an appreciably slower process. Being formed, it starts to decompose, and the low-temperature oxidation mechanism (see Fig. 1) does not appear. In this case, ignition proceeds as a single-stage process.

At a lower temperature $T_0 = 900$ K, the reaction rates of monodecomposition and oxidation of n-decane (these reactions belong to classes 1 and 2, respectively) become almost identical. Therefore, the concentrations of light alkyl radicals and HO_2 are identical at the initial stage at $0 < t < 10^{-8}$ sec. The formation of alkylperoxide radicals $C_{10}H_{20}O_2$ (class 8) becomes more significant; their concentration is practically equal to the concentration of light olefins. It initiates the development of the chain process through the low-temperature mechanism (see Fig. 1). This process is described by reactions of classes 9–12. As a result, $OC_{10}H_{19}OOH$ radicals form; their concentration reaches the highest value in the time interval $3 \cdot 10^{-6} \leqslant t < 3 \cdot 10^{-5}$ sec.

Nevertheless, despite a drastic increase in the concentration of active radicals, carriers of the chain process, in this time interval, the number of these radicals is obviously insufficient to provide ignition (the mole fraction is within 0.02%). At $t > 3 \cdot 10^{-5}$ sec, intense recombination of these radicals begins, which results in the increase in temperature up to 1000 K at $t = 1.5 \cdot 10^{-4}$ sec. At this temperature, the high-temperature mechanism also contributes significantly to the chain process development, and the mixture is ignited at $t = 2.5 \cdot 10^{-4}$ sec.

With a further decrease in the initial temperature down to $T_0 = 750$ K, n-$C_{10}H_{22}$ oxidation proceeds much faster than its monomolecular decomposition. Therefore, the concentrations of $C_{10}H_{21}O_2$ and HO_2 noticeably exceed the concentrations of alkyl radicals even at the initial stage of the process ($0 \leqslant t < 10^{-8}$ sec), and the low-temperature oxidation mechanism dominates, which is evidenced by the drastic increase in the concentration of the $OC_{10}H_{19}OOH$ radical up to the time instant $t = 3 \cdot 10^{-4}$ sec. This radical prevails in the time interval $2.10^{-6} \leqslant t < 3 \cdot 10^{-4}$ sec. Though its mole fraction reaches 0.16%, which is noticeably greater than that even at $T_0 = 900$ K, no ignition occurs at $t = 3 \cdot 10^{-4}$ sec. Intense recombination of active radicals leads to an increase in temperature, which reaches 990 K at $t = 4 \cdot 10^{-4}$ sec, and ignition occurs at $t = 5 \cdot 10^{-4}$ sec.

At an even lower temperature $T_0 = 650$ K, the formation of active radicals, carriers of the chain mechanism, follows the low-temperature mechanism and proceeds noticeably slower than that at $T_0 = 750$ K. The induction time in this case is appreciably greater as well ($\tau_{\text{ind}} = 5 \cdot 10^{-3}$ sec).

Thus, we can conclude that cold-flame phenomena occur in the course of n-decane oxidation through the low-temperature mechanism. They are caused by energy release due to intense recombination of radicals, which leads to an increase in gas temperature and to changes in the character of chain reactions when the high-temperature oxidation mechanism becomes dominating.

It is worth noting another important and interesting fact associated with low-temperature ignition of the n-$C_{10}H_{22}/O_2$(air) mixture, which is often ignored in modeling ignition of heavy hydrocarbons in the low-temperature region: with decreasing T_0, the final temperature of combustion products T_e also decreases, but the fraction of the chemical energy of the species that can be transformed to thermal energy increases.

PYROLYSIS OF *n*-DECANE

Pyrolysis of all hydrocarbons is accompanied by a decrease in temperature and appearance of new species; the most significant of them are alkenes C_nH_{2n} ($n = 2, 3$), and also H_2, CH_4, and C_2H_2. A detailed analysis of n-decane pyrolysis was performed in [30], based on results of experiments carried out in a flow reactor where the time histories of various products of pyrolysis at a certain distance from the reactor entrance were measured. It should be noted that data obtained in flow reactors are widely used for testing kinetic models. In comparisons of calculated and experimental results, however, the non-perfect character of mixing in the flow reactor should be taken into account. Therefore, many researchers use a time shift in testing models, thus, trying to avoid errors associated with considerable difficulties in calculating edge effects in the input region of the reactor [30]. The reference point is usually chosen as a point where the concentration of the initial species (in the case considered, n-decane) reaches 50% of its initial concentration. The same procedure was used in this work. Figure 11 shows the dependences $\gamma_i(t)$ for the basic species formed during n-decane pyrolysis at $p_0 = 1$ atm and $T_0 = 1060$ K, which were measured in [30] and were calculated by the present model and by the model developed in [30]. Both the calculations and experiments show that the dominating product of n-decane decomposition is ethylene; the concentrations of other alkenes (C_3H_6, C_4H_8, and C_5H_{10}) are noticeably lower. Apart from alkenes, noticeable amounts of methane and acetylene are also formed (note that the H_2 concentration was not measured in this experiment). In the case of 50% conversion of n-decane, the fraction of all above-mentioned compounds reaches ap-

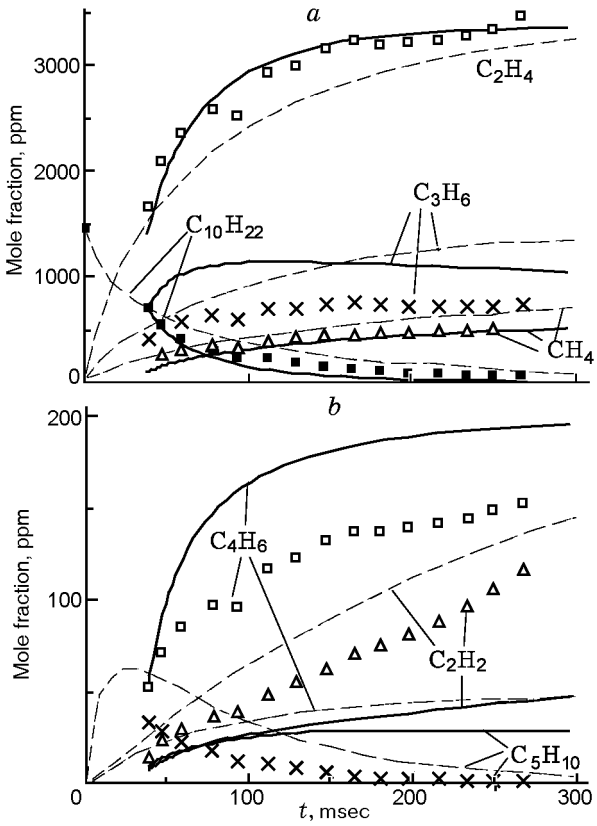

Fig. 11. Mole fractions of species obtained in experiments [30] (points) and calculated by the model developed in [30] (dashed curves) and by the model proposed in this paper (solid curves) for the case of n-$C_{10}H_{22}$ pyrolysis in a flow reactor at $p = 1$ atm, $T_0 = 1060$ K, and 1456 ppm n-$C_{10}H_{22}$.

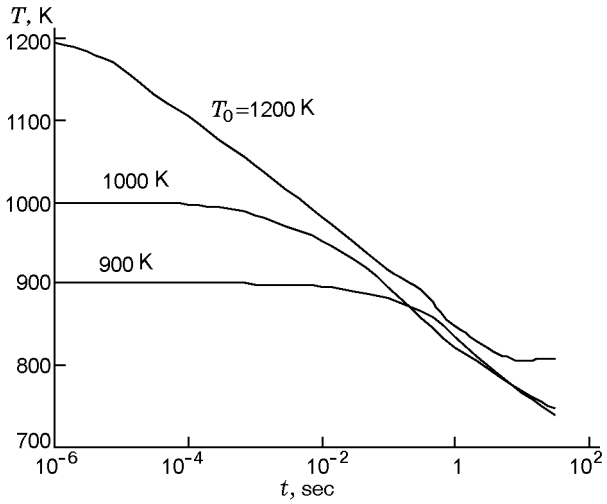

Fig. 12. Behavior of temperature during n-$C_{10}H_{22}$ pyrolisis in an adiabatic reactor at $p_0 = 1$ atm and $T_0 = 1200$, 1000, and 900 K.

proximately 80% of all hydrocarbon species, which are pyrolysis products. It is seen in Fig. 11 that good agreement is observed between the experimental data and the results calculated by the model developed in [30] and by our model for the basic products of pyrolysis. The concentrations of important components, such as C_2H_4 and CH_4, are accurately reproduced by calculations. This fact suggests that this kinetic model can be used to analyze the time evolution of various pyrolysis products and the degree of n-decane conversion as functions of gas temperature.

Figures 12 and 13 show the dependences $T(t)$ and $\gamma_i(t)$ at $p_0 = 1$ atm and $T_0 = 1200$, 1000, and 900 K for the case of n-decane pyrolysis in an adiabatic reactor. It follows from these figures that an increase in T_0 leads, first, to faster decomposition of n-$C_{10}H_{22}$ and, second, to faster reaching the maximum concentrations of C_2H_4, C_3H_6, C_4H_8, C_5H_{10}, and H_2 in pyrolysis products. At the same time, the CH_4 concentration monotonically increases during n-decane pyrolysis at all initial temperatures. Two stages in the formation of n-decane pyrolysis products are observed. At the first (earlier) stage of the decomposition process (its duration depends on the value of T_0), C_2H_4, H_2, and C_3H_6 form. After reaching the maximum values, the concentrations of these species decrease, while the concentrations of C_5H_{10} and CH_4 continue to grow. At the second stage, C_5H_{10} and CH_4 dominate in pyrolysis products. The higher the value of T_0, the greater the CH_4 concentration in pyrolysis products. The higher the value of T_0, the greater the degree of n-decane decomposition and the more pronounced the decrease in temperature. For these reasons, fuels based on n-decane can be considered as good coolants for cooling combustors of jet engines. In this case, however, it should be borne in mind that the composition of pyrolysis products essentially depends on the fuel residence time in the cooling duct and on the temperature of the combustor walls, i.e., the fuel composition may become cardinally changed at the exit from the cooling system and may alter the basic parameters characterizing the combustion efficiency.

CONCLUSIONS

A lumped kinetic model has been developed to describe n-decane oxidation and pyrolysis. It includes both the high-temperature and low-temperature mechanisms of chain process development. This model offers an accurate description of experimental data on ignition delay times in n-$C_{10}H_{22}/O_2$(air) mixtures at high ($T_0 =$

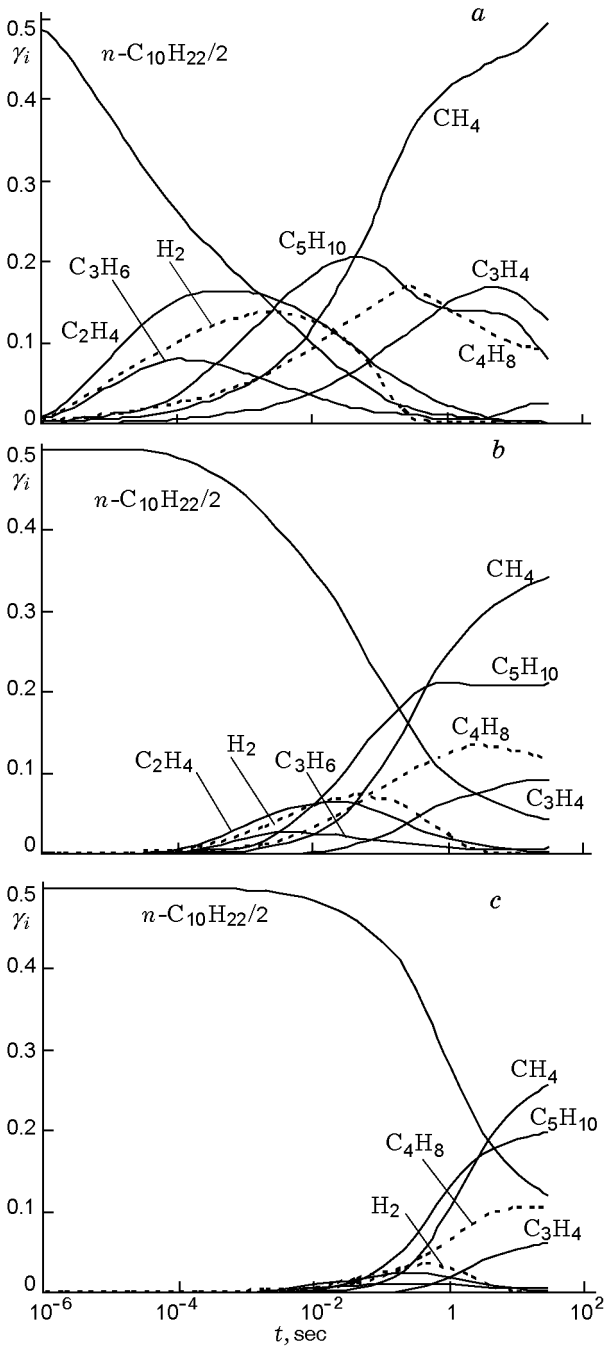

Fig. 13. Mole fractions γ_i of the basic species formed during n-decane pyrolysis in an adiabatic reactor at $p_0 = 1$ atm and $T_0 = 1200$ (a), 1000 (b), and 900 K (c).

1000–1800 K) and low ($T_0 = 650$–1000 K) temperatures in a wide range of initial pressures ($p_0 = 1.2$–80 atm) and equivalence ratios ($\phi = 0.5$–3). The induction times predicted by the present kinetic model differ from the measured values by less than 25% in the entire considered ranges of parameters and compositions of the mixture. Detailed reaction mechanisms built up to now by other researchers cannot ensure this level of accuracy (2-fold to 2.5-fold differences are observed in the low-temperature region even for the most advanced models). The present model also reproduces properly the temporal profile of the OH concentration, which was measured during n-decane ignition behind the reflected shock wave, and the time histories of species concentrations in the course of n-$C_{10}H_{22}$ pyrolysis at atmospheric pressure, which were obtained in experiments in a flow reactor.

It was found that a two-stage mode of ignition occurs at low temperatures of the n-$C_{10}H_{22}/O_2$(air) mixture. At the first stage of chain process development, the active radicals are formed by the low-temperature mechanism: something like a precursor of ignition occurs. Nevertheless, the number of active radicals formed at this stage is insufficient to provide the ignition. The second stage is driven by intense recombination of radicals formed previously and by an increase in temperature up to 950–970 K (it is this stage that is responsible for the appearance of the so-called cold-flame phenomena). After that, the process follows two mechanisms (low-temperature and high-temperature), and ignition of the mixture occurs at the end of this stage.

This work was supported by the Russian Foundation for Basic Research Grant Nos. 08-08-00839 and 09-08-92006-NNS) and by the Federal Purpose Program "Science-Educational Manpower of Innovational Russia" (State Contract No. 02.740.11.0074).

REFERENCES

1. M. Frenklach and D. E. Bornside, "Shock-initiated ignition in methane-propane mixtures," *Combust. Flame*, **56**, No. 1, 1–27 (1984).
2. K. M. Leung and R. P. Lindstedt, "Detailed kinetic modeling of C_1—C_3 alkane diffusion flames," *Combust. Flame*, **102**, Nos. 1/2, 129–160 (1995).
3. H. G. Dautov and A. M. Starik, "On the problem of choosing a kinetic scheme for the homogeneous reaction of methane with air," *Kinet. Catal.*, **38**, No. 2, 185–208 (1997).
4. M. V. Petrova and F. A. Williams, "A small detailed chemical-kinetic mechanism for hydrocarbon combustion," *Combust. Flame*, **144**, No. 3, 526–544 (2006).
5. S. Kojima, "Detailed modeling of n-butane autoignition chemistry," *Combust. Flame*, **99**, Nos. 1/2, 87–136 (1994).
6. A. M. Starik, N. S. Titova, and L. S. Yanovskii, "Kinetics of the oxidation of the products from the thermal destruction of C_3H_8 and C_4H_{10} in the mixture with air," *Kinet. Catal.*, **40**, No. 1, 7-22 (1999).

7. A. Chakir, M. Bellimam, J. C. Boettner, and M. Cathonnet, "Kinetic study of *n*-heptane oxidation," *Int. J. Chem. Kinet.*, **24**, No. 4, 385–410 (1992).
8. R. P. Lindstedt and L. Q. Maurice, "Detailed kinetic modeling of *n*-heptane combustion," *Combust. Sci. Technol.*, **107**, No. 4, 317–353 (1995).
9. H. J. Curran, P. Gaffuri, W. J. Pitz, and C. K. Westbrook, "A comprehensive modeling study of iso-octane oxidation," *Combust. Flame*, **129**, No. 3, 253–280 (2002).
10. N. A. Slavinskaya and A. M. Starik, "Kinetic mechanisms of ignition of isooctane–air mixtures," *Combust., Expl., Shock Waves*, **40**, No. 1, 36–56 (2004).
11. C. Doute, J.-L. Delfau, R. Akrich, and C. Vovelle, "Chemical structure of atmospheric pressure premixed *n*-decane and kerosene flames," *Combust. Sci. Technol.*, **106**, Nos. 4–6, 327–344 (1995).
12. P. Dagaut, M. Reuillon, M. Cathonnet, and D. Voisin, "High pressure oxidation of normal decane and kerosene in dilute conditions from low to high temperature," *J. Chem. Phys.*, **92**, 47–76 (1995).
13. A. Ristori, P. Dagaut, and M. Cathonnet, "The oxidation of *n*-hexadecane: Experimental and detailed kinetic modeling," *Combust. Flame*, **125**, No. 3, 1128–1137 (2001).
14. E. Ranzi, A. Frassoldati, S. Granata, and T. Faravelli, "Wide-range kinetic modeling study of the pyrolysis, partial oxidation, and combustion of heavy *n*-alkanes," *Ind. Eng. Chem. Res.*, **44**, No. 14, 5170–5183 (2005).
15. R. P. Lindstedt and L. Q. Maurice, "Detailed chemical-kinetic model for aviation fuels," *J. Propulsion Power*, **16**, No. 2, 187–195 (2000).
16. M. A. Mawid and B. Sekar, "Development of a detailed JP-8/Jet-A chemical kinetic mechanism for high pressure conditions in gas turbine combustors," in: *Proc. of GT2006*, ASME Paper No. GT2006-90478 (2006).
17. M. Kraft, P. Maigaard, F. Mauss, M. Christensson, and B. Johansson, "Investigation of combustion emissions in a homogeneous charge compression injection engine: Measurements and a new computational model," *Proc. Combust. Inst.*, **28**, 1195–1201 (2000).
18. P. Dagaut, "On the kinetics of hydrocarbons oxidation from natural gas to kerosene and diesel fuel," *Phys. Chem. Chem. Phys.*, **4**, 2079–2094 (2002).
19. P. Dagaut, M. Reuillon, J.-C. Boettner, and M. Cathonnet, "Kerosene combustion at pressures up to 40 atm: experimental study and detailed chemical kinetic modelling," *Proc. Combust. Inst.*, **25**, 919–926 (1994).
20. P. Dagaut, M. Reuillon, and M. Cathonnet, "High pressure oxidation of liquid fuels from low to high temperature. 3. *n*-Decane," *Combust. Sci. Technol.*, **103**, 349–359 (1994).
21. C. K. Westbrook, W. J. Pitz, O. Herbinet, H. J. Curran, and E. J. Silke, "A comprehensive detailed chemical kinetic reaction mechanism for combustion of *n*-alkane hydrocarbons from *n*-octane to *n*-hexadecane," *Combust. Flame*, **156**, No. 1, 181–199 (2009).
22. E. Olchanski and A. Burcat, "Decane oxidation in a shock tube," *Int. J. Chem. Kinet.*, **38**, No. 12, 703–713 (2006).
23. D. C. Horning, "A Study of high-temperature autoignition and thermal decomposition of hydrocarbons," Ph.D. Thesis, Department of mechanical engineering, Stanford University, USA (2001).
24. D. C. Horning, D. F. Davidson, and R. K. Hanson, "Study of the high-temperature autoignition of *n*-alkane/O_2/Ar mixtures," *J. Propuls. Power*, **18**, No. 2, 363–371 (2002).
25. N. Blin-Simiand, F. Jorand, K. Sahetchian, et al., "Hydroperoxides with zero, one, two or more carbonyl groups formed during the oxidation of *n*-dodecane," *Combust. Flame*, **126**, Nos. 1/2, 1524–1532 (2001).
26. D. F. Davidson, J. T. Herbon, D. C. Horning, and R. K. Hanson, "OH concentration time histories in *n*-alkane oxidation," *Int. J. Chem. Kinet.*, **33**, No. 12, 775–783 (2001).
27. U. Pfahl, K. Fieweger, and G. Adomeit, "Self-ignition of diesel-relevant hydrocarbon-air mixtures under engine conditions," *Proc. Combust. Inst.*, **26**, 781–789 (1996).
28. V. P. Zhukov, V. A. Sechenov, A. Yu. Starikovskii, "Autoignition of *n*-decane at high pressure," *Combust. Flame*, **153**, Nos. 1/2, 130–136 (2008).
29. A. J. Dean, O. G. Penyazkov, K. L. Sevruk, and B. Varatharajan, "Autoignition of surrogate fuels at elevated temperatures and pressures," *Proc. Combust. Inst.* **31**, 2481–2488 (2007).
30. S. P. Zeppieri, S. D. Klotz, and F. L. Dryer, "Modeling concepts for larger carbon number alkanes: a partially reduced skeletal mechanism for *n*-decane oxidation and pyrolysis," *Proc. Combust. Inst.*, **28**, 1587–1595 (2000).
31. F. Battin-Leclerc, R. Fournet, P. A. Glaude, et al., "Modeling of the gas-phase oxidation of *n*-decane from 550 to 1600 K," *Proc. Combust. Inst.* **28**, 1597–1605 (2000).
32. G. Bikas and N. Peters, "Kinetic modeling of *n*-decane combustion and autoignition," *Combust. Flame*, **126**, Nos. 1/2, 1456–1475 (2001).
33. S. M. Aceves, D. L. Flowers, C. K. Westbrook, et al., "A multi-zone model for prediction of HCCI combustion and emissions," SAE Paper No. 2000-01-0327 (2000).
34. W. Easley, A. Agarwal, and G. A. Lavoie, "Modeling of HCCI combustion and emissions using detailed chemistry," SAE Paper No. 2001-01-1029 (2001).
35. A. Violi, S. Yan, E. G. Eddings, et al., "Experimental formulation and kinetic model for JP-8 surrogate mixtures," *Combust. Sci. Technol.*, **174**, 399–417 (2002).

36. A. Agosta, N. P. Cernansky, D. L. Miller, et al., "Reference components of jet fuels: kinetic modeling and experimental results," *Exp. Therm. Fluid. Sci.*, **28**, 701–708 (2004).
37. L. V. Bezgin, V. I. Kopchenov, A. M. Starik, and N. S. Titova, "Modeling studies of ignition and combustion of propane and the products of its thermal destruction in a supersonic air flow," in: G. Roy, S. Frolov, and J. Sinibaldi (eds.), *Pulsed and Continuous Detonations*, Torus, Moscow (2006), pp. 301–307.
38. A. Patel, S.-C. Kong, and R. D. Reitz, "Development and validation of reduced reaction mechanism for HCCI engine simulations," SAE Paper No. 2004-01-0558 (2004).
39. Q. Tang and S. B. Pope, "Implementation of combustion chemistry by in situ adaptive tabulation of rate-controlled constrained equilibrium manifolds," Proc. Combust. Inst. **29**, 1411–1417 (2002).
40. B. Bhattacharjee, D. A. Schwer, P. I. Barton, and W. H. Green, "Optimally-reduced kinetic models: reaction elimination in large-scale kinetic mechanisms," *Combust. Flame*, **135**, No. 3, 191–208 (2003).
41. J. F. Griffiths, K. J. Hughes, M. Schreiber, and C. Poppe, "A unified approach to the reduced kinetic modeling of alkane combustion," *Combust. Flame*, **99**, Nos. 3/4, 533–540 (1994).
42. J. Zheng, D. L. Miller, W. Yang, and N. Cernansky, "Prediction of pre-ignition reactivity and ignition delay for HCCI using a reduced chemical kinetic model," SAE Paper No. 2001-01-1025 (2001).
43. A. Bourdon, G. Rymer, and R. Wanker, "Optimization of 5-Step kinetic scheme for HCCI applications," SAE Paper No. 2004-01-0559 (2004).
44. J. Zheng, D. L. Miller, and N. P. Cernansky, "A global reaction model for the HCCI combustion process," SAE Paper No. 2004-01-2950 (2004).
45. A. M. Starik, B. I. Lukhovitskii, and N. S. Titova, "Mechanism of the initiation of combustion in $CH_4(C_2H_2)/Air/O_3$ mixtures by laser excitation of the O_3 molecules," *Kinet. Catal.*, **48**, No. 3, 348-366 (2007).
46. R. P. Lindstedt and L. Q. Maurice, "Detailed chemical kinetic modelling of toluene combustion," *Combust. Sci. Technol.*, **120**, 119–167 (1996).
47. H. J. Curran, available at: http://www-cms.llnl.gov/combustion/combustion_home.html.
48. A. Burcat and B. Ruscic, available at: ftp://ftp.technion.ac.il/pub/supported/aetdd/ thermodynamics.
49. S. W. Benson, *Thermochemical Kinetics*, John Wiley and Sons (1976).
50. W. C. Gardiner, *Combustion Chemistry*, Springer-Verlag (1984).